ACSNANO
www.acsnano.org
ARTICLE

Lift-Off Free Fabrication Approach for Periodic Structures with Tunable Nano Gaps for Interdigitated Electrode Arrays

Stefan Partel,[*,†,‡] Can Dincer,[‡,§] Stephan Kasemann,[†] Jochen Kieninger,[‡] Johannes Edlinger,[†] and Gerald Urban[‡,§]

[†]Vorarlberg University of Applied Sciences, 6850 Dornbirn, Austria
[‡]Department of Microsystem Engineering (IMTEK), University of Freiburg, 79110 Freiburg, Germany
[§]Freiburg Materials Research Center (FMF), University of Freiburg, 79104 Freiburg, Germany

ABSTRACT: **We report a simple, low-cost and lift-off free fabrication approach for periodic structures with adjustable nanometer gaps for interdigitated electrode arrays (IDAs). It combines an initial structure and two deposition process steps; first a dielectric layer is deposited, followed by a metal evaporation. The initial structure can be realized by lithography or any other structuring technique (*e.g.*, nano imprint, hot embossing or injection molding). This method allows the fabrication of nanometer sized gaps and completely eliminates the need for a lift-off process. Different substrate materials like silicon, Pyrex or polymers can be used. The electrode gap is controlled primarily by sputter deposition of the initial structure, and thus, adjustable gaps in the nanometer range can be realized independently of the mask or stamp pattern. Electrochemical characterizations using redox cycling in ferrocenemethanol (FcMeOH) demonstrate signal amplification factors of more than 110 together with collection factors higher than 99%. Furthermore, the correlation between the gap width and the amplification factor was studied to obtain an electrochemical performance assessment of the nano gap electrodes. The results demonstrate an exponential relationship between amplification factor and gap width.**

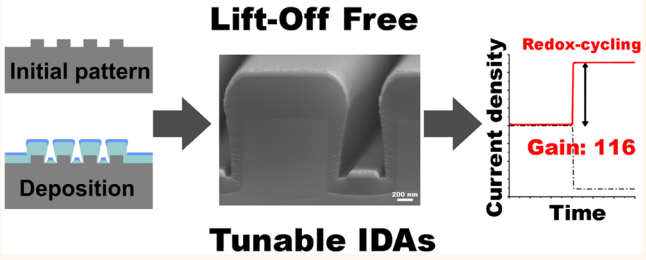

KEYWORDS: *interdigitated electrode array, lift-off free fabrication, tunable nano gaps, amperometric biosensor, electrochemical impedance spectroscopy, redox cycling*

Biosensors can be classified by their transducer principles, and the most common one is the electrochemical biosensor.[1] It converts an analyte concentration into an electrical signal using a biocomponent, typically an enzyme. To enhance the sensitivity of the conventional electrodes and to obtain low capacitive currents and small resistance effects, interdigitated electrode arrays (IDAs) are often applied in electrochemistry with thin-film electrodes.[2−10] When the electrode size shrinks down to submicron and nanometer sizes, more advanced manufacturing technologies are required such as e-beam, focused ion beam, nano imprint, phase shift lithography, interference lithography, deep ultraviolet-, extreme ultraviolet- or projection photolithography.[3,11−22] However, these processes are more expensive, and some are more time-consuming and cause specific requirements to substrate and photoresist. One limitation of the mass-fabrication of highly sensitive realizing biosensor devices is the ability to miniaturize the transduction principle in a cost-effective manner.[23] The fabrication of IDAs in nanometer dimensions comprises in principle a combination of high resolution patterning method and a subsequent lift-off process. In all of these techniques the most critical step is the lift-off process, which has to be successful without any redeposition or residues to guarantee high yields. This can be achieved when the profile of the pattern shows a negative flank (slope) angle or undercut, otherwise the side slopes get coated during evaporation with the conductive electrode material. Consequently, specific requirements regarding the photoresist profile are mandatory. The demands on process reliability and stability are increasing with the shrinking gaps between the fingers. Thinking of electrochemical methods like redox cycling, one important aspect is that the electrode width plays a secondary role for a high signal amplification factor. Primarily, the gap between the electrodes determines the amplification.[8,12,13,24,25] On the basis of this perception and our empirical knowledge a novel fabrication process was developed. The presented method is a

Received: October 12, 2015
Accepted: December 1, 2015

DOI: 10.1021/acsnano.5b06405
ACS Nano XXXX, XXX, XXX−XXX

combination of an initial structure and two deposition processes. An initial structure can be created by lithography or any other structuring technique with rather low resolution (1 μm l/s) followed by two deposition processes to form the undercut and the electrodes (see Figure 1).

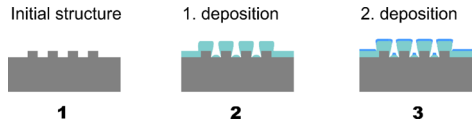

Figure 1. Fabrication process: (1) Forming of the initial structure; (2) 1. Deposition process (sputter deposition) to form the undercut; (3) 2. Deposition process (evaporation) to form the electrodes.

The fabrication method completely eliminates the lift-off process and does not depend on high end structuring principles. This makes it most suitable for mass production. A detailed description of the fabrication process can be found in the Materials and Methods.

RESULTS

The presented fabrication process allows the realization of electrode gaps in the sub 100 nm range. The electrode gap can be adjusted without changing the mask design, only by varying the thickness of the sputter deposited dielectric layer. Different thicknesses of SiO_2 layers were tested as well as varying the pitch of the initial structures (see Figure 2c). Gap sizes down to 43 nm have been fabricated successfully (see Figure 2b). For this small gap size, the initial structure exhibits a pitch of 1.44 μm. Subsequently, a 700 nm thick SiO_2 layer was sputtered to form the gap of 43 nm between electrodes.

For our first electrochemical measurements an initial pattern with 2 μm pitch (1 μm gap and 1 μm feature) was chosen. Subsequently, a layer of 500 nm SiO_2 was sputter deposited followed by a 100 nm Au evaporation. An electrode gap of ~160 nm was achieved, measured with SEM after electrochemical characterization.

A 100 nm thick layer of Au was chosen to define the interdigitated electrodes (see Figure 2a). Figure 3 shows the undercut profile and the successful separation of the electrodes. The characteristic formation of an undercut profile is used to obtain an electrical separation of the top and bottom surface. For the sputter deposited 500 nm SiO_2 layer an undercut of more than 100 nm can be observed. This is more than sufficient for a complete separation of the electrodes.

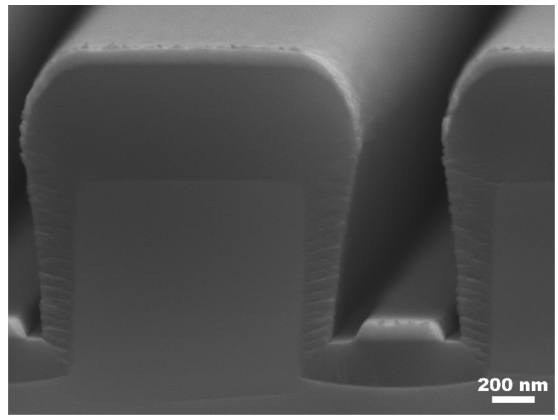

Figure 3. Cross section of a 1 μm l/s structure etched 1 μm deep into silicon. A 500 nm SiO_2 layer was sputtered, followed by a 100 nm thick Au evaporation resulting in a final gap size of 340 nm.

Different investigations were done to verify the formation of the undercut profile for submicron structures. The correlation between initial structure and final gap size is of interest as well

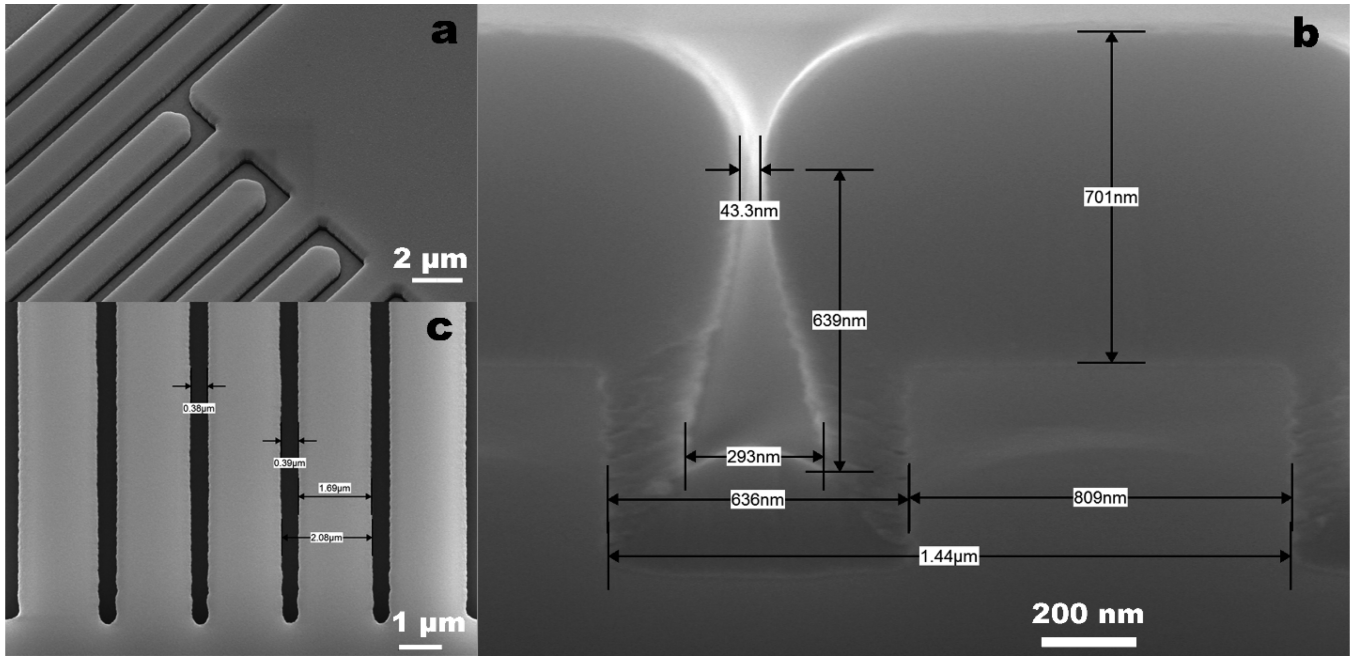

Figure 2. (a) SEM image of the formed undercut profile after 500 nm SiO_2 sputtering and 100 nm Au evaporation. The initial dry etched structure has a gap of 1 μm and a period of 2 μm. (b) Cross section of a 700 nm line and space (l/s) structure with 700 nm SiO_2. The minimum distance is ~43 nm on top and ~300 nm on the bottom. (c) 1 μm l/s test pattern after deposition of 500 nm SiO_2. The gap is ~390 nm with an electrode size of ~1.7 μm.

DOI: 10.1021/acsnano.5b06405
ACS Nano XXXX, XXX, XXX−XXX

as the dimension of the formed undercut. For the verification, the deposited dielectric layer was kept constant and exhibits a thickness of 400 nm (Figure 5). The structures were etched 1 μm deep into silicon and were kept constant for all samples. The aspect ratio dependent etch rate (ARDE) which describes the etch rate change for different trench widths was taken into account for the characterization.[26,27] Figure 4 shows important

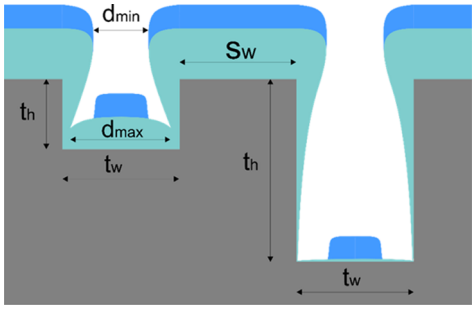

Figure 4. Schematic of the formed undercut profile with the most important parameters for the characterization at low and high aspect ratio.

parameters for the characterization of the formed undercut profile. The initial feature is defined by trench height (t_h) and trench width (t_w). The structure width (s_w) is not influencing the formation of the undercut profile. The minimum distance (d_{min}) and the maximum distance (d_{max}) after SiO_2 deposition are measured to calculate the undercut angle. In addition, the influence of the aspect ratio on the profile shape is illustrated in Figure 4.

The relation between the initial feature size (t_w) and the resulting distances were measured and are reported in Figure 5.

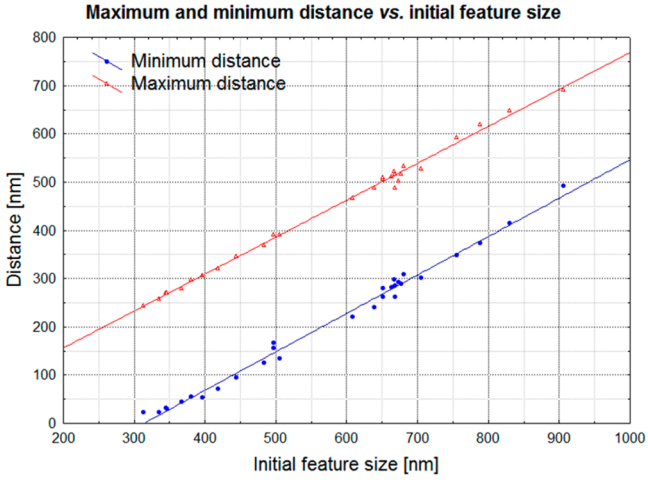

Figure 5. Measurement data for a 1 μm deep dry etched structure and the resulting minimum gap size formed by sputtering of 400 nm SiO_2. The blue dots are the measured distance at the bottom of the structure with the largest distance. The red triangles are the measured distance on the top of the structure.

The distance between the elevated initial structures is named as initial feature size in the diagram (abscissa) and corresponds to t_w. The minimum and maximum distance (ordinate) describes the resulting distance between the two structures after SiO_2 deposition. The blue dots show the measured distance on the bottom of the resulting structure (d_{max}) and the red triangles the upper distance d_{min} (which is related to the effective electrode distance). For example, an initial structure has an etched feature size of 500 nm. After deposition of 400 nm SiO_2, the gap between the structures will be 150 nm. With the second deposition process the upper distance decreases further. For instance, evaporating 100 nm Au results in a ~10 nm reduction. For this feature an undercut of around 100 nm per side was measured. The diagram also shows that the dimension of the formed undercut is nearly constant, independent of t_w. At higher aspect ratios less deposited material will be entering the clearance between the structures, which results in lower film thickness on the bottom of the trench (compare Figure 3 and Figure 6).

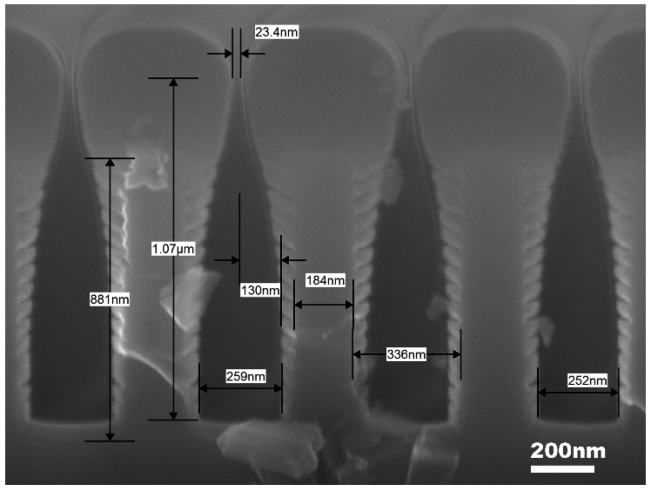

Figure 6. SEM image of the cross section of a test pattern with high aspect ratio. The initial elevated structure has a width of about 180 nm and is separated by about 340 nm. The 400 nm SiO_2 layer results in a gap of 23 nm.

Initial structures down to around 180 nm width separated by gaps of about 340 nm were fabricated. The etch depth (t_h) was about 880 nm resulting in an aspect ratio of 5:1 (trench height to structure width). For the formation of the undercut profile the trench height to trench width is more characteristic (aspect ratio of 2.6:1). Because of the higher aspect ratio and the small distance between the elevated structures the penetration depth of the deposited material is lower. The resulting shape is shown in Figure 6. The electrode gap is 23 nm and a very thin layer of SiO_2 is covering the bottom of the initial structure. Clearly evident are the sidewall ripples of the initial structure which are formed in the dry etching step (gas chopping).[28] These ripples get more intense during SiO_2 deposition because the deposited material accumulates on the hillock. This phenomenon does not influence the undercut profile in a negative way. Quite in reverse: The ripples are causing a columnar growth of the SiO_2 and the spacing between the columns would prevent an electrical contact in case they would get coated with Au. However, at very high aspect ratios the thickness of the SiO_2 layer between the columns becomes thinner and in worst case results in uncovered Si. During electrochemical measurements this circumstance could enable a leakage current between the fingers through the Si substrate.

For interpretation of undercut profile formation the aspect ratio of initial trench height to trench width is more representative (instead of the commonly used ratio of height to elevated structure width), since the width of the elevated

DOI: 10.1021/acsnano.5b06405
ACS Nano XXXX, XXX, XXX−XXX

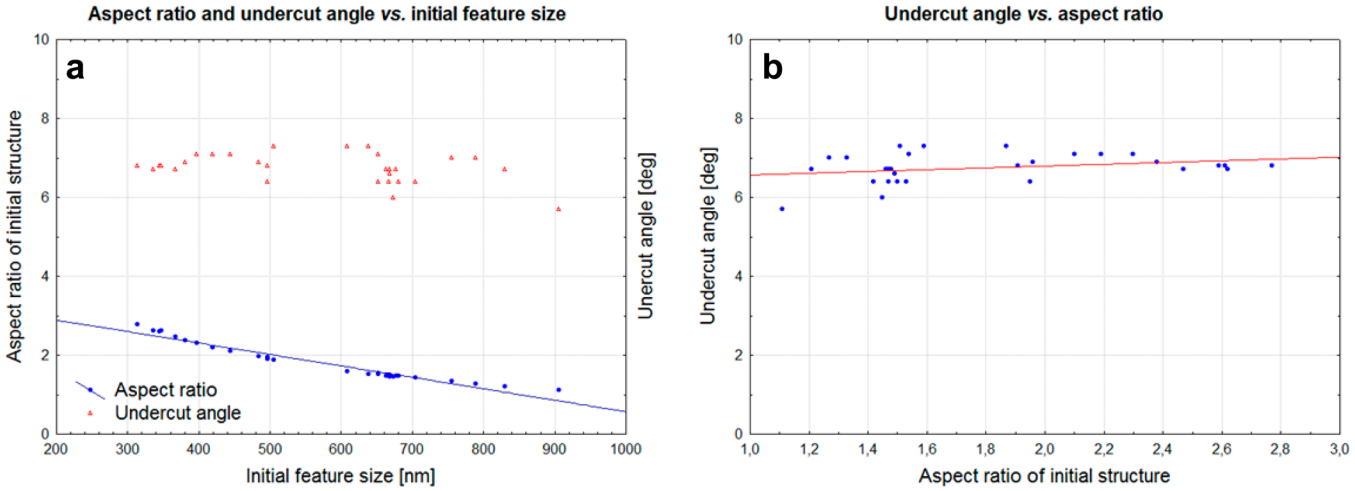

Figure 7. Diagram (a) shows the measured aspect ratio of the initial structure *vs* the initial feature size (blue dots). The red triangles are showing the undercut angle *vs* the initial feature size. Diagram (b) shows the undercut angle *vs* the trench aspect ratio of the initial structure.

structure has no influence on the profile shape. Plotting the trench aspect ratio and the undercut angle *vs* the initial feature size it becomes obvious, that the undercut angle is nearly independent of the initial feature size (see Figure 7a, red dots). For all features measured in the submicron region the undercut angle is between about 6° to about 7.5°. Furthermore, the diagram shows that the undercut angle is nearly independent of the trench aspect ratio. The undercut angle *vs* aspect ratio plot confirms the assumption of the independency (Figure 7b). Nevertheless, it is observed that at higher aspect ratios the undercut profile is more shifted to a bottle like shape as illustrated in the SEM image in Figure 6. For a 300 nm initial trench width the SiO_2 layer on the bottom exhibits a thickness of 50 nm. The SiO_2 sidewall thickness is even lower. In comparison, a structure with 610 nm initial trench width shows an SiO_2 bottom thickness of 100 nm and SiO_2 sidewall thickness of about 85 nm, with the sidewall thickness increasing more rapidly in the top region of the structure.

Electrochemical Characterization. In redox cycling at IDAs, the redox active species oxidized at one finger electrode (generator) diffuses most probably to the neighboring electrode (collector) applied to a reduction potential where it is reduced again back to the initial form. The result is an electrochemical amplification of both the generator and collector current signals. This "feedback effect" is also known as the generator/collector mode in the context of the scanning electrochemical microscopy (SECM) and has been extensively studied in the past.[29−31]

The results of the electrochemical characterization are summarized in Figure 8. First, cyclic voltammograms (CVs) have been recorded in normal mode (by polarizing only one pair of IDA) to identify the redox potentials of FcMeOH and then, in scanning mode (by scanning the first IDA pair while applying on the second pair to a fixed reduction potential) to demonstrate the feasibility of redox cycling.

$$FcMeOH + e^- \leftrightarrow FcMeOH^+$$

As displayed in Figure 8b, the use of FcMeOH as redox system leads to a stable signal amplification by redox cycling. Here, at the first working electrode (generator) a CV was recorded with the second working electrode (collector) set to a potential of 0 V allowing the simultaneous reduction of $FcMeOH^+$ back to FcMeOH.

Amperometric measurements using the fabricated gold IDAs with 160 nm electrode gap were carried out in 0.1 M PBS with 1 mM FcMeOH as shown in Figure 8c. In the redox cycling mode, one of IDA fingers was polarized to an oxidation potential of +500 mV *vs* Ag/AgCl as the first working electrode (WE1), while the other finger to a reduction potential of 0 V *vs* Ag/AgCl as the second working electrode (WE2). Comparing with the normal mode, an increase in signal sensitivity was observed about 116 times for the redox cycling. Moreover, the resulted collection factor (the ratio between the absolute values of the collector and the generator currents[32−34]) was approximately 99.5%. Besides, the effect of the electrode gap size on the electrochemical amplification was investigated to demonstrate the applicability of the fabrication process. IDAs with different electrode gap widths including 160, 180, 195, 200, 220, 250, 270 nm and 1 μm were employed in duplicates. The amplification factors calculated from these measurements are displayed in Figure 8d. Here, the well-known exponential behavior[32−34] of the redox cycling amplification is clearly observed. As described in Aoki *et al.*,[34] the redox cycling currents at IDAs under steady-state conditions are inversely proportional to the gap width between the IDA electrodes and displays an exponential behavior. The achieved signal amplification compared to the conventional amperometry is mainly caused by the enhanced mass transport of the redox active substances. A decrease in the size of the electrode gap leads to a shortening of the diffusion length of electroactive species and thus an increase in electrochemical amplification factor.

DISCUSSION

Traditional fabrication methods define the critical structures by lithography.[11,12,35] In our novel approach the critical dimension (gap between the electrodes) is determined not primarily by photolithography, but by the precise and easily controllable sputter deposition process. The thickness of the deposited layer can be controlled within the nanometer range. This allows a very precise adjustment of the gap between the electrode structures. Furthermore, the sputtering process enables a variation of the gap width without a change in the mask design. This means different gap sizes can be realized without additional costs, even in the sub 100 nm range. The reproducibility is primarily reliant on the initial structure

DOI: 10.1021/acsnano.5b06405
ACS Nano XXXX, XXX, XXX−XXX

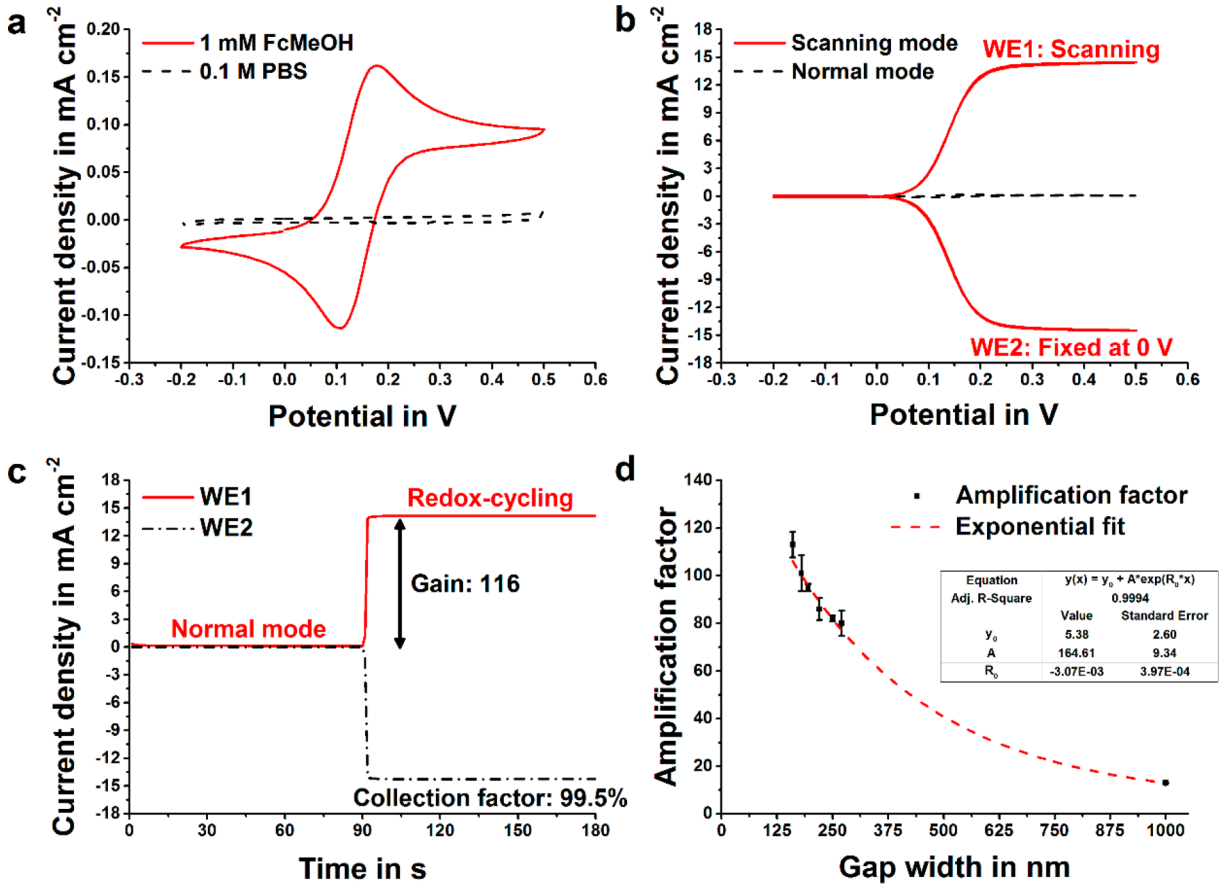

Figure 8. (a) Cyclic voltammograms in 0.1 M phosphate buffered saline (PBS) and 1 mM FcMeOH at the gold working electrode with a scan rate of 100 mV s^{-1}. All applied potentials are reported with respect to the on-chip silver/silver chloride pseudoreference electrode. (b) CVs in 0.1 M PBS with 1 mM FcMeOH using normal mode (black curve) and scanning mode (red curve) with redox cycling, applying 0 V at the second working electrode. (c) Amperometric measurements using the fabricated gold IDAs with 160 nm electrode gap in 0.1 M PBS with 1 mM FcMeOH. The first working electrode (WE1, red curve) was set at an oxidation potential of 500 mV *vs* Ag/AgCl, while the second working electrode (WE2, black curve) at a reduction potential of 0 V *vs* Ag/AgCl. Comparing to the normal mode, an amplification factor of 116 and a collection factor of 99.5% was demonstrated by redox cycling. (d) The correlation between the gap width and the amplification factor shows an exponential increase of the electrochemical response using redox cycling. An electrochemical amplification can be obtained by decreasing the size of the gap between the finger electrodes.

which was fabricated by mask aligner lithography with subsequent dry etching. The resolution of mask aligner lithography strongly depends on the contact between mask and wafer. For high yield and precise control of resolution, projection lithography, laser direct writing, hot embossing or injection molding are preferred.

Another outstanding advantage of this fabrication method is the elimination of the lift-off process. The lift-off process is one of the critical steps in nanoelectrode fabrication. First, it is difficult to produce sub 100 nm features with sufficient undercut profile. Second, eventual short-circuits will most probably be generated during the lift-off step. By completely eliminating the lift-off process, the necessary undercut profile is generated automatically and no metal residue is generated. Therefore, any short-circuit between the electrodes can be avoided.

The results of the electrochemical characterization demonstrate that the presented electrode design manufactured applying the novel fabrication method is very well suitable for redox cycling measurements. Furthermore, this method enables to control the gap width precisely and easily (even in nm range) in comparison to the state of art fabrication techniques.[36−39] Subsequently, redox cycling measurements on the gold IDAs with different electrode gaps were performed in ferrocenemethanol. Consequently, signal amplification factors of about 116 and collection factors of more than 99% were observed for the IDAs with 160 nm electrode gap. Moreover, the study of the correlation between the gap width and the amplification factor proves an exponential behavior of the measured electrochemical response which matches well with the theory of redox cycling.[32−34]

CONCLUSION

In conclusion, a simple and low-cost fabrication method for the IDAs with adjustable nano gaps is introduced offering high amplification factors in redox cycling measurements. The presented method is a combination of an initial structure and two deposition processes. The initial structure can be created by lithography or any other structuring technique with lower resolution (micrometer range). For instance, the initial structure can be produced with injection molding, which makes the process suitable for mass production. Even patterned photoresist as an initial structure would be applicable. The choice of substrate material is relatively uncritical (only temperature stability in the deposition process plays a role) and thus, polymers can easily be employed as a substrate. With

DOI: 10.1021/acsnano.5b06405
ACS Nano XXXX, XXX, XXX−XXX

this fabrication sequence, it is possible to generate gaps in the range of sub 100 nm without any lift-off process (a gap size of 23 nm is presented in this paper). Therefore, very high yield and precision is possible. Another major advantage is that the gap between the electrodes can be controlled primarily by sputter deposition, thus the gap can be adjusted almost independently of the mask pattern. Different gap widths can be obtained with a single mask later on. This way, determination of the optimum gap size for a specific application gets very simple. With the invented fabrication technique we demonstrated an amplification factor of 116 together with a collection factor of 99.5%. This is, to the best of our knowledge, the highest amplification factor achieved by redox cycling so far. Furthermore, an exponential behavior of the measured electrochemical signals was clearly observed by decreasing the gap width between the finger structures. The employment of IDA structures with nano gaps is not only limited to amperometric techniques in electrochemistry. Also for electrochemical impedance spectroscopy (EIS) for label-free detection the nano gaps are of high interest. The great increase in detection ability using nano interdigitated electrodes in biomolecular and cellular analysis are well-known known and frequently reported.[20,40,41] Our fabrication method has the ability to bring electrochemical sensing innovations to mass production.

MATERIALS AND METHODS

The presented method is a combination of an initial structure and two deposition processes. Figure 9 shows the simple method to fabricate

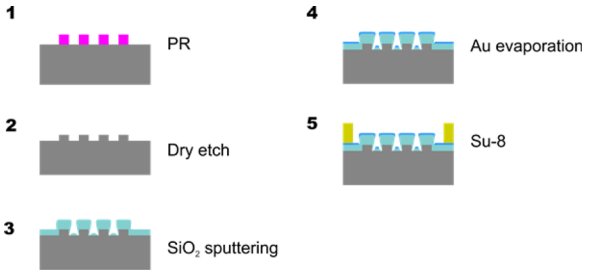

Figure 9. Fabrication process chain: (1) Patterning with photoresist (PR); (2) dry etching into silicon; (3) sputtering of the dielectric layer; (4) evaporating of the electrode material; (5) defining electrode area and the contact pads.

the nano IDAs. The undercut for electrode definition is automatically formed during sputtering process. Assistant features are integrated in mask design to ensure a sufficient separation of the electrodes. Primarily, these features are necessary for outer electrodes and connector areas. A sufficient undercut is formed only if a nearby structure is present. The die size is 20 × 5.5 mm and includes two fully functional IDA chips. The large size of the chip facilitates a comfortable implementation of microfluidics and easy sample handling.[39,42] The initial structure for the finger pattern is 1 μm electrode size with a 1 μm distance to each other. There are 300 finger pairs with finger length of 149 μm resulting in an effective sensing/electrode area of 0.175 mm^2. Furthermore, for each chip, a reference electrode with an area of 0.258 mm^2 is implemented as well as a third electrode acting as counter electrode.

For the chip fabrication, silicon as a substrate and photoresist AZ 701 MiR (purchased from Microchemicals GmbH, Germany) as a masking layer for dry etching of silicon were used. The thickness of the photoresist was 760 nm measured with a Dektak 8 (Bruker, USA). The wafer was exposed with a SUSS mask aligner MA6 (SUSS MicroTec AG, Germany) and MO Exposure Optics[43] in vacuum contact mode. For the development of the photoresist the developer AZ 726 MIF was used to dissolve the exposed areas. The initial structure size was 1 μm electrode width and 1 μm gap between the finger electrodes. The structures were etched 1 μm deep into silicon by a dry etching process with gas chopping technique[28,44] (SF_6, C_4F_8) for 52 s. This step was performed on a deep reactive ion etching (DRIE) ICP system Adixon AMS100 (Alcatel Vacuum technology, France). After transferring the pattern into silicon the photoresist was removed using oxygen plasma. To form the undercut profile, a 700 nm thick SiO_2 layer was sputtered (LLS EVO, Oerlikon Balzers, Liechtenstein). Subsequently, a 100 nm thick layer of Au was evaporated in high vacuum (Univex 500, Oerlikon Leybold Vacuum GmbH, Germany) to define the electrodes. Because of the undercut formed during the sputtering process, the electrodes are electrically separated. After evaporation the wafer was spin-coated with SU8−3005 with a final thickness of 5 μm to define the electrode areas and the contact pads. An on-chip reference electrode is provided by electrodeposition of silver (Ag) and afterward partial electrochemical conversion of the silver to silver chloride (AgCl). The wafer was singularized into individual sensor chips by fs-laser dicing (3DMicromac, Germany). Scanning electron microscopy (SEM) images and measurements were taken with FEI XL30 ESEM FEG (FEI, USA) and JEOL 7100F (JEOL Ltd., Japan), equipment. The characterization of the sputtered SiO_2 layer was performed by spectroscopic ellipsometry on a VASE system (J.A. Woollam Co., Inc., USA). The final gold IDAs with different electrode gaps were characterized using 0.1 M phosphate buffered saline (PBS) solution with 0.1 M NaCl containing 1 mM FcMeOH under steady-state conditions (no flow). The resistance between the interdigitated electrode structures was verified to be higher than 20 MΩ in its dry-state prior to any experiment. All electrochemical measurements were done using a bipotentiostat (CompactStat.e, Ivium Technologies B.V., Netherlands). On-chip silver/silver chloride (Ag/AgCl) and a gold electrode were employed as reference and counter electrode, respectively.

AUTHOR INFORMATION

Corresponding Author

*E-mail: stefan.partel@fhv.at.

Notes

The authors declare no competing financial interest.

ACKNOWLEDGMENTS

We would like to thank Matthias Domke (Vorarlberg University of Applied Sciences, Josef-Ressel-Centre) for his support on laser dicing.

REFERENCES

(1) *BioMEMS*; Urban, G. A., Ed.; Microsystems; Springer: Dordrecht, 2006.

(2) Kätelhön, E.; Krause, K. J.; Mathwig, K.; Lemay, S. G.; Wolfrum, B. Noise Phenomena Caused by Reversible Adsorption in Nanoscale Electrochemical Devices. *ACS Nano* **2014**, *8*, 4924−4930.

(3) Ma, C.; Contento, N. M.; Gibson, L. R.; Bohn, P. W. Redox Cycling in Nanoscale-Recessed Ring-Disk Electrode Arrays for Enhanced Electrochemical Sensitivity. *ACS Nano* **2013**, *7*, 5483−5490.

(4) Elsholz, B.; Nitsche, A.; Achenbach, J.; Ellerbrok, H.; Blohm, L.; Albers, J.; Pauli, G.; Hintsche, R.; Wörl, R. Electrical Microarrays for Highly Sensitive Detection of Multiplex PCR Products from Biological Agents. *Biosens. Bioelectron.* **2009**, *24*, 1737−1743.

(5) Nebling, E.; Grunwald, T.; Albers, J.; Schäfer, P.; Hintsche, R. Electrical Detection of Viral DNA Using Ultramicroelectrode Arrays. *Anal. Chem.* **2004**, *76*, 689−696.

(6) Dharuman, V.; Grunwald, T.; Nebling, E.; Albers, J.; Blohm, L.; Hintsche, R. Label-Free Impedance Detection of Oligonucleotide Hybridisation on Interdigitated Ultramicroelectrodes Using Electrochemical Redox Probes. *Biosens. Bioelectron.* **2005**, *21*, 645−654.

(7) Kraus, S.; Kleines, M.; Albers, J.; Blohm, L.; Piechotta, G.; Püttmann, C.; Barth, S.; Nähring, J.; Nebling, E. Quantitative

DOI: 10.1021/acsnano.5b06405
ACS Nano XXXX, XXX, XXX−XXX

Measurement of Human Anti-HCV Core Immunoglobulins on an Electrical Biochip Platform. *Biosens. Bioelectron.* **2011**, *26*, 1895−1901.
(8) Singh, K. V.; Whited, A. M.; Ragineni, Y.; Barrett, T. W.; King, J.; Solanki, R. 3D Nanogap Interdigitated Electrode Array Biosensors. *Anal. Bioanal. Chem.* **2010**, *397*, 1493−1502.
(9) Güder, F.; Yang, Y.; Krüger, M.; Stevens, G. B.; Zacharias, M. Atomic Layer Deposition on Phase-Shift Lithography Generated Photoresist Patterns for 1D Nanochannel Fabrication. *ACS Appl. Mater. Interfaces* **2010**, *2*, 3473−3478.
(10) Nam, S.-W.; Lee, M.-H.; Lee, S.-H.; Lee, D.-J.; Rossnagel, S. M.; Kim, K.-B. Sub-10-Nm Nanochannels by Self-Sealing and Self-Limiting Atomic Layer Deposition. *Nano Lett.* **2010**, *10*, 3324−3329.
(11) Skjolding, L. H. D.; Spegel, C.; Ribayrol, A.; Emnéus, J.; Montelius, L. Characterisation of Nano-Interdigitated Electrodes. *J. Phys.: Conf. Ser.* **2008**, *100*, 052045.
(12) Ueno, K.; Hayashida, M.; Ye, J.-Y.; Misawa, H. Fabrication and Electrochemical Characterization of Interdigitated Nanoelectrode Arrays. *Electrochem. Commun.* **2005**, *7*, 161−165.
(13) Samarao, A. K.; Rust, M. J.; Ahn, C. H. Rapid Fabrication of a Nano Interdigitated Array Electrode and Its Amperometric Characterization as an Electrochemical Sensor. *IEEE Sens. 2007, [IEEE Conf. Sens.], 6th* **2007**, 644−647.
(14) Santschi, C.; Jenke, M.; Hoffmann, P.; Brugger, J. Interdigitated 50 Nm Ti Electrode Arrays Fabricated Using XeF2 Enhanced Focused Ion Beam Etching. *Nanotechnology* **2006**, *17*, 2722−2729.
(15) Lanyon, Y.; Arrigan, D. Recessed Nanoband Electrodes Fabricated by Focused Ion Beam Milling. *Sens. Actuators, B* **2007**, *121*, 341−347.
(16) Beck, M.; Persson, F.; Carlberg, P.; Graczyk, M.; Maximov, I.; Ling, T. G. I.; Montelius, L. Nanoelectrochemical Transducers for (bio-) Chemical Sensor Applications Fabricated by Nanoimprint Lithography. *Microelectron. Eng.* **2004**, *73*−*74*, 837−842.
(17) Sandison, M. E.; Cooper, J. M. Nanofabrication of Electrode Arrays by Electron-Beam and Nanoimprint Lithographies. *Lab Chip* **2006**, *6*, 1020.
(18) Yokoo, A.; Namatsu, H.; Oda, M. Nanoelectrode Lithography. *MRS Online Proc. Libr.* **2006**, DOI: 10.1557/PROC-0961-O10-01.
(19) Städler, B.; Solak, H. H.; Frerker, S.; Bonroy, K.; Frederix, F.; Vörös, J.; Grandin, H. M. Nanopatterning of Gold Colloids for Label-Free Biosensing. *Nanotechnology* **2007**, *18*, 155306.
(20) Van Gerwen, P.; Laureyn, W.; Laureys, W.; Huyberechts, G.; Op De Beeck, M.; Baert, K.; Suls, J.; Sansen, W.; Jacobs, P.; Hermans, L.; et al.*et al.* Nanoscaled Interdigitated Electrode Arrays for Biochemical Sensors. *Sens. Actuators, B* **1998**, *49*, 73−80.
(21) Stuerzebecher, L.; Fuchs, F.; Zeitner, U. D.; Tuennermann, A. High-Resolution Proximity Lithography for Nano-Optical Components. *Microelectron. Eng.* **2015**, *132*, 120−134.
(22) Weichelt, T.; Vogler, U.; Stuerzebecher, L.; Voelkel, R.; Zeitner, U. D. Resolution Enhancement for Advanced Mask Aligner Lithography Using Phase-Shifting Photomasks. *Opt. Express* **2014**, *22*, 16310.
(23) Grieshaber, D.; MacKenzie, R.; Vörös, J.; Reimhult, E. Electrochemical Biosensors - Sensor Principles and Architectures. *Sensors* **2008**, *8*, 1400−1458.
(24) Heo, J. I.; Shim, D. S.; Teixidor, G. T.; Oh, S.; Madou, M. J.; Shin, H. Carbon Interdigitated Array Nanoelectrodes for Electrochemical Applications. *J. Electrochem. Soc.* **2011**, *158*, 76−80.
(25) Singh, K. V.; Bhura, D. K.; Nandamuri, G.; Whited, A. M.; Evans, D.; King, J.; Solanki, R. Nanoparticle-Enhanced Sensitivity of a Nanogap-Interdigitated Electrode Array Impedimetric Biosensor. *Langmuir* **2011**, *27*, 13931−13939.
(26) Rangelow, I. W. Critical Tasks in High Aspect Ratio Silicon Dry Etching for Microelectromechanical Systems. *J. Vac. Sci. Technol., A* **2003**, *21*, 1550.
(27) Blauw, M. A.; Zijlstra, T.; Bakker, R. A.; van der Drift, E. Kinetics and Crystal Orientation Dependence in High Aspect Ratio Silicon Dry Etching. *J. Vac. Sci. Technol., B: Microelectron. Process. Phenom.* **2000**, *18*, 3453.
(28) Rangelow, I. W. Reactive Ion Etching for High Aspect Ratio Silicon Micromachining. *Surf. Coat. Technol.* **1997**, *97*, 140−150.
(29) Bard, A. J.; Fan, F. R. F.; Kwak, J.; Lev, O. Scanning Electrochemical Microscopy. Introduction and Principles. *Anal. Chem.* **1989**, *61*, 132−138.
(30) Bard, A. J.; Mirkin, M. V.; Unwin, P. R.; Wipf, D. O. Scanning Electrochemical Microscopy. 12. Theory and Experiment of the Feedback Mode with Finite Heterogeneous Electron-Transfer Kinetics and Arbitrary Substrate Size. *J. Phys. Chem.* **1992**, *96*, 1861−1868.
(31) Kwak, J.; Bard, A. J. Scanning Electrochemical Microscopy. Theory of the Feedback Mode. *Anal. Chem.* **1989**, *61*, 1221−1227.
(32) Niwa, O.; Morita, M.; Tabei, H. Electrochemical Behavior of Reversible Redox Species at Interdigitated Array Electrodes with Different Geometries: Consideration of Redox Cycling and Collection Efficiency. *Anal. Chem.* **1990**, *62*, 447−452.
(33) Bard, A.; Crayston, J.; Kittlesen, G.; Varco Shea, T.; Wrighton, M. Digital Simulation of the Measured Electrochemical Response of Reversible Redox Couples at Microelectrode Arrays: Consequences Arising from Closely Spaced Ultramicroelectrodes. *Anal. Chem.* **1986**, *58*, 2321−2331.
(34) Aoki, K.; Morita, M.; Niwa, O.; Tabei, H. Quantitative Analysis of Reversible Diffusion-Controlled Currents of Redox Soluble Species at Interdigitated Array Electrodes under Steady-State Conditions. *J. Electroanal. Chem. Interfacial Electrochem.* **1988**, *256*, 269−282.
(35) Cohen, A. E.; Kunz, R. R. Large-Area Interdigitated Array Microelectrodes for Electrochemical Sensing. *Sens. Actuators, B* **2000**, *62*, 23−29.
(36) del Campo, F. J.; Abad, L.; Illa, X.; Prats-Alfonso, E.; Borrisé, X.; Cirera, J. M.; Bai, H.-Y.; Tsai, Y.-C. Determination of Heterogeneous Electron Transfer Rate Constants at Interdigitated Nanoband Electrodes Fabricated by an Optical Mix-and-Match Process. *Sens. Actuators, B* **2014**, *194*, 86−95.
(37) Hu, C.-F.; Wang, J.-Y.; Liu, Y.-C.; Tsai, M.-H.; Fang, W. Development of 3D Carbon Nanotube Interdigitated Finger Electrodes on Polymer Substrate for Flexible Capacitive Sensor Application. *Nanotechnology* **2013**, *24*, 444006.
(38) Shim, J. S.; Rust, M. J.; Ahn, C. H. A Large Area Nano-Gap Interdigitated Electrode Array on a Polymer Substrate as a Disposable Nano-Biosensor. *J. Micromech. Microeng.* **2013**, *23*, 035002.
(39) Partel, S.; Kasemann, S.; Choleva, P.; Dincer, C.; Kieninger, J.; Urban, G. A. Novel Fabrication Process for Sub-Micron Interdigitated Electrode Arrays for Highly Sensitive Electrochemical Detection. *Sens. Actuators, B* **2014**, *205*, 193−198.
(40) Zou, Z.; Kai, J.; Rust, M. J.; Han, J.; Ahn, C. H. Functionalized Nano Interdigitated Electrodes Arrays on Polymer with Integrated Microfluidics for Direct Bio-Affinity Sensing Using Impedimetric Measurement. *Sens. Actuators, A* **2007**, *136*, 518−526.
(41) Zhu, X.; Ahn, C. H. Electrochemical Determination of Reversible Redox Species at Interdigitated Array Micro/Nanoelectrodes Using Charge Injection Method. *IEEE Trans. Nanobiosci.* **2005**, *4*, 164−169.
(42) Partel, S.; Mayer, M.; Hudek, P.; Dinçer, C.; Kieninger, J.; Urban, G. A.; Motzek, K.; Matay, L. Fabrication Process Development for a High Sensitive Electrochemical IDA Sensor. *Microelectron. Eng.* **2012**, *97*, 235−240.
(43) Voelkel, R.; Vogler, U.; Bich, A.; Pernet, P.; Weible, K. J.; Hornung, M.; Zoberbier, R.; Cullmann, E.; Stuerzebecher, L.; Harzendorf, T.; et al.*et al.* Advanced Mask Aligner Lithography: New Illumination System. *Opt. Express* **2010**, *18*, 20968−20978.
(44) Volland, B.; Shi, F.; Hudek, P.; Heerlein, H.; Rangelow, I. W. Dry Etching with Gas Chopping without Rippled Sidewalls. *J. Vac. Sci. Technol., B: Microelectron. Process. Phenom.* **1999**, *17*, 2768.

DOI: 10.1021/acsnano.5b06405
ACS Nano XXXX, XXX, XXX−XXX